Reduced Order Models for Droplet Evaporation with Internal Circulation

K. Kroenlein, A. Kazakov, and F.L. Dryer
Mechanical and Aerospace Engineering, Princeton University, Princeton, NJ 08540

Introduction

Internal circulation generated by relative gas/drop velocities has a significant and well-documented effect on evaporation and combustion of liquid droplets (Law, 1982; Faeth, 1983; Dwyer, 1989). Large Reynolds numbers have typically been of interest because of relevance to sprays. Internal circulatory motions in small (~20 μm diameter) droplets are quickly damped by viscosity but can contribute significantly to overall behaviors due to augmented heat and mass transfer during their short evaporative histories. Even when no relative gas/drop motion is initially present, internal liquid motions can be imparted during droplet generation. Moreover, internal motions also can arise from fluid instabilities as a result of surface tension gradients induced by circumferential surface temperature variations, and for multi-component droplets, circumferential surface composition. There have been several recent numerical and experimental studies further exploring these phenomena (Niazmand et al., 1994; Shih and Megaridis, 1995; Dwyer and Shaw, 2001; Savino and Fico, 2004), but none have addressed conditions that include local gas phase heat release (combustion).

In the large (~1 mm diameter) droplets typically investigated in microgravity research, even under quiescent gas/drop conditions, internal motions have been observed to persist over the entire droplet burning lifetime (Choi and Dryer, 2001). The effects of internal liquid phase motions on mass and energy transfer have been included in numerical sphero-symmetric modeling by utilizing an "effective liquid phase Lewis number which was much larger than that associated with the thermophysical properties of the liquid components (Marchese and Dryer, 1997). More recently, similar modifications were required to model falling drop experimental results for ethanol droplet combustion (Kazakov et al. (2003). To include liquid phase internal motions in a fully coupled, discrete manner results in a computationally constrained formulation that likely will require simplifications in other sub-model components for gas phase transport, combustion chemistry, sooting, radiation coupling, and phase transformation. The long term goal addressed to which the present effort contributes is to develop a more rigorous reduced-dimensional (e.g., quasi-one-dimensional) formulation that successfully emulates the important effects of multi-dimensional internal liquid phase motion. In order to more precisely address spherosymmetric microgravity combustion and to include slow gas/drop convection, it is important to account for internal phase liquid motions more rigorously.

The calibration and validation of any reduced model requires availability of detailed (theoretical and/or experimental) data. In the case of internal liquid motions inside the droplet, the direct experimental data are very scarce at best, and clearly insufficient in terms of the resolution required. Here we develop a new detailed two-dimensional computational model that can be applied to generate the required calibration information for both liquid droplet evaporation and combustion cases. The presented detailed two-dimensional computational model fully resolves the flow field for isolated droplets, and accounts for variable thermo-physical properties and free surface boundary conditions. Viscous and thermo-capillary effects are also included so that the results can be applied to conditions important under microgravity isolated droplet combustion conditions with and without slow gas/drop convection.

Numerical Formulation

The computational system was formulated using a first-order finite volume method. The equations of conservation of mass, momentum and energy were initially expressed as:

$$\frac{\partial}{\partial t}\iiint_V \rho dV + \oiint_A \vec{u}\cdot\nabla\rho dA = 0$$

$$\frac{\partial}{\partial t}\iiint_V \rho\vec{u} dV + \oiint_A \vec{u}\cdot\nabla\rho\vec{u} dA = \oiint_A P\vec{n} dA - \oiint_A \mu\left(\nabla\vec{u}\right)\cdot\vec{n} dA$$

$$\frac{\partial}{\partial t}\iiint_V \rho c T dV + \oiint_A \vec{u}\cdot\nabla\rho c T dA = -\oiint_A \lambda\left(\nabla T\right)\cdot\vec{n} dA$$

where in addition to explicit coupling of the energy equation and the flow via convection there is an implicit coupling via the evaluation of transport parameters and liquid density. Liquid density, viscosity, thermal conductivity, and surface tension were evaluated using experimentally based correlations for specific liquids taken from the compilation of Daubert and Danner (1989). The properties of *n*-decane were utilized for the results presented here.

We used a solution procedure based upon the SIMPLER algorithm outlined by Patankar (1980). A Poisson equation with modifications to account for variations in liquid density with temperature was used to solve for the pressure field. A pressure corrector equation was applied to enforce local mass conservation, and staggered grids were employed for both radial and angular velocities. The above conservation equations were adapted to an axisymmetric spherical system, allowing for dynamic boundary motion. The surfaces of each control volume were allowed to move to fix the outer-most control volume boundary on the regressing liquid surface, with the constraint that the relative spacing between the inner nodes remains constant.

In order to increase computational accuracy in the vicinity of the surface, as well as to provide more accurate gradient evaluation in all cells, the control volumes were constrained to contain equal volumes. The characteristic diffusive lengths used in determining gradients were defined based upon the centroids of each control volume. Since the value of each property identified with a particular control volume is intended to represent an average value for that property within the grid cell, the centroids most accurately represent the locations with that value of the property.

In order to simulate a combustion environment in the surrounding gas-phase, a five-equation algebraic model was used, based upon a derivation similar to that for the classic "d^2-law" (Turns, 2000). Separate constant (non-unity) values for the inner and outer flow region Lewis numbers, along with averaged values for the remaining parameters, and an infinite value for the Damköhler number were assumed. The four equations of conservation of fuel mass, oxidizer mass, energy at the flame sheet and energy at the liquid-solid interface can be expressed as:

$$\frac{\dot{m}_s}{4\pi R^2} = \left[\rho D_{oxidizer}\ln\left(1+\nu^{-1}\right) - \rho D_{fuel}\ln\left(1-Y_{F,s}\right)\right]/R$$

$$\frac{r_f}{R} = 1 - \frac{D_{fuel}\ln\left(1-Y_{F,s}\right)}{D_{oxidizer}\ln\left(1+\nu^{-1}\right)}$$

$$\frac{T_s - T_f}{\exp\left(-\frac{c_p}{\lambda}\frac{\dot{m}_s}{4\pi R^2}R\right) - \exp\left(-\frac{c_p}{\lambda}\frac{\dot{m}_s}{4\pi R^2}\frac{R}{r_f}R\right)} - \frac{T_\infty - T_f}{1-\exp\left(-\frac{c_p}{\lambda}\frac{\dot{m}_s}{4\pi R^2}R\right)} = \frac{c_p/\Delta h_c}{\exp\left(-\frac{c_p}{\lambda}\frac{\dot{m}_s}{4\pi R^2}\frac{R}{r_f}R\right)}$$

$$T_s = T_f + \left[1-\exp\left(-\frac{c_p}{\lambda}\frac{\dot{m}_s}{4\pi R^2}\left(\frac{R}{r_f}-1\right)R\right)\right]\left[\lambda\left.\frac{\partial T}{\partial r}\right|_{liquid} + h_{fg}\left(T_s\right)\left(\frac{\dot{m}_s}{4\pi R^2} - \rho_g\dot{R}\right)\right]\Bigg/ c_p\frac{\dot{m}_s}{4\pi R^2}$$

The last equation is determines the surface mass fraction of fuel, $Y_{F,s}$, as a function of vapor pressure and and an assumed mean molecular weight of the post-combustion gases. Both the partial pressure and latent heat of vaporization were evaluated as functions of surface temperature with correlations from Daubert and Danner (1989). This system was solved iteratively for surface temperature and the Stefan

flux at each time step. The Stefan flux, or, more accurately, the Stefan flux per unit surface area, was then converted to a mass vaporization rate per unit surface area, providing the mass sink term for each surface location and the temperature to be used as the energy source. The instantaneous surface temperature was used to calculate the instantaneous local surface tension, and surface tension gradients determined the surface momentum source in the angular momentum equation.

These five equations require four parameters, ρD_{fuel}, $\rho D_{oxidizer}$ $(1+\nu^{-1})$, c_p/λ, and c_p, which are not known *a priori*, but could be provided with significant numerical analysis. We calibrated these parameters through one-dimensional droplet combustion simulations performed with an in-house code (Cho et al., 1992) that has been utilized extensively (e.g. Choi and Dryer, 2001; Kazakov et al., 2003). Calculations were performed using *n*-decane properties from Daubert and Danner (1989) and the *n*-decane chemical kinetic model of Zhao et al. (2005). The predicted values for burning rate, droplet surface temperature, droplet standoff ratio and peak flame temperature were then used to evaluate the above parameters.

Preliminary Computational Results

Simulations were performed for a number of cases involving *n*-decane droplets. Droplets with Peclet numbers (based upon initial surface velocity) of 0, 2, and 4 were simulated at initial droplet radii of 10 μm, 100 μm, and 1 mm. These Peclet numbers were selected based upon the characteristic Peclet numbers found in conventional spray combustion and droplet sizes characteristic of both spray and fundamental isolated droplet combustion studies. A sample mesh deployment used in the simulations is presented in Fig. 1. The total number of grid cells used in the simulations was 1105, 45 in radial and 25 in angular direction, respectively. A single computational run took approximately 3 hours on an Athlon XP 2800+ Linux workstation.

The incompressible solution of Rybczynski and Hadamard (Happel and Brenner, 1965) for a spherical liquid droplet in a gas moving with constant free-stream velocity was applied as an initial condition (Fig. 2). In all cases, the initial velocity fields decayed quite rapidly to simple expanding droplets due to viscous dissipation and surface forces from thermal gradients. After less than 2.5% of the total burning time of the droplet, all observed flow in the system consisted of the effects of expansion from the penetrating thermal wave (Fig 3). Without a persistent tangential driving force provided at the droplet surface, in the form of an gas/drop relative velocity or solutal Marangoni instabilities in multi-component droplets for example, all internal motions were quickly damped.

A sample droplet burning history is presented in Figure 4. The standoff ratio for the flame is accurately reproduced during the first 75% of the burning history in comparison with the one-dimensional simulation, particularly considering the simplicity of the surface model. As expected, the rapid increase in flame standoff ratio near burnout is not reproduced because the surface model contains no chemical influence. Thus, as the droplet begins to undergo extinction-type behavior, the simple surface heating model no longer tracks the decay in chemical conversion. The model also reproduces an initial heating transient followed by an approach to a constant slope in the diameter squared time history profile, as discussed by Law (1982). As the system remains conductively limited during the entire burning history (Figure 5), the slope of the diameter-squared curve continuously increases with time. In the very beginning of the burning history (Figure 6), one can see a small increase in diameter associated with the heating of the outermost layers of liquid before there is sufficient vapor pressure to support rapid combustion.

Summary

Internal circulation generated by relative gas/drop velocities, droplet deployment, or Marangoni effects have significant effects on droplet burning properties in both practical and fundamental droplet combustion. Modeling these effects under combustion conditions with realistic properties is important to interpreting fundamental microgravity combustion observations as well as developing sub-models

appropriate for practical combustion situations involving sprays. A quasi-one-dimensional representation of liquid phase internal circulation effects that accurately reproduces the multi-dimensional case would permit inclusion internal circulation effects in models with detailed descriptions for gas phase transport, chemical kinetics, sooting, and radiation. In order to calibrate, such a model, a two-dimensional test problem has been developed. The assumptions for developing the model were discussed, and some initial results based upon calculations have been presented, and calibration of a one-dimensional representation of the results is underway.

Acknowledgements

This work was supported under NASA Grants NCC3-735 and NNC04AA66A.

References

Choi, M.Y., and Dryer, F.L. (2001) *Microgravity Combustion: Fire in Free Fall* (Howard Ross, ed.) Academic Press.

Daubert, T.E., and Danner, R.P. (1989), *Physical and Thermodynamic Properties of Pure Chemicals*, Hemisphere.

Dwyer, H.A., (1989) Prog. Energy Combust. Sci. 15, 131.

Dwyer, H.A., and Shaw, B.D. (2001) Combust . Sci. Tech. 162, 331.

Faeth, G.M., (1983) Prog. Energy Combust. Sci. 9, 1.

Happel, J and Brenner, H. (1965) *Low Reynolds Number Hydrodynamics*. Prentice-Hall

Kazakov, A., Conley, J., and Dryer, F.L. Combust. Flame Combust. Flame 134, 301.

Law, C.K. (1982) Prog. Energy Combust. Sci. 8, 171.

Marchese, A.J., and Dryer, F.L. (1997) Combust. Sci. Tech. 124, 371.

Niazmand, H., Shaw, B.D., Dwyer, H.A., and Aharon, I. (1994) Combust. Sci. Tech 103, 219.

Patankar, S.V. (1980) *Numerical Heat Transfer and Fluid Flow*, McGraw-Hill.

Savino, R. and Fico, S. (2004) Phys. Fluids 16, 3738.

Shih, A.T. and Megaridis, C.M. (1996) Int. J. Heat Mass Transfer 39, 247.

Sirignano, W.A. (1983) Prog. Energy Combust. Sci. 9, 291.

Turns, S.R. (2000) *An Introduction to Combustion: Concepts and Applications*. McGraw-Hill.

Zhao, Z., Li, J., Kazakov, A., Zeppieri, S.P., and Dryer, F.L. (2005) Combust. Sci. Tech. 177, 89.

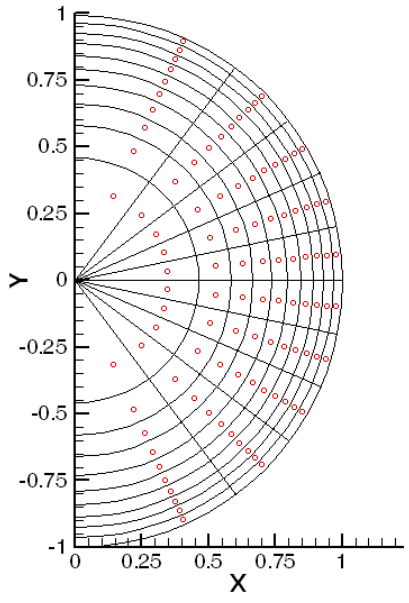

Figure 1. Low-resolution example of mesh deployment used in two-dimensional simulations (a finer grid used in actual production runs is not shown fro visual clarity). The circles indicate the locations of centroids within each grid cell.

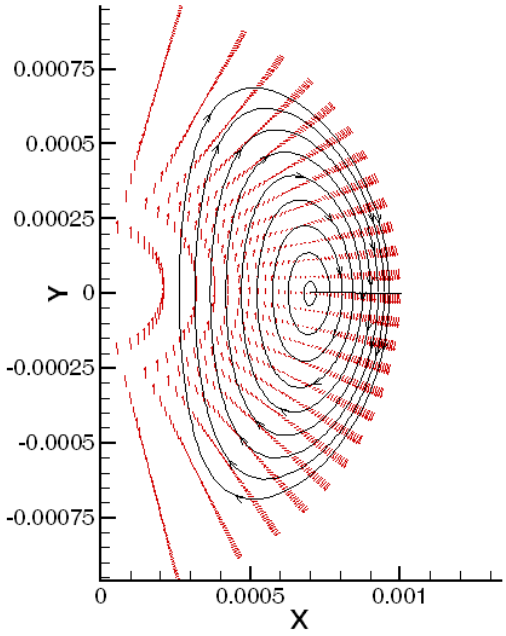

Figure 2. Initial condition of velocity field from the analytical solution of Rybczynski and Hadamard (R = 1 mm, Pe = 4).

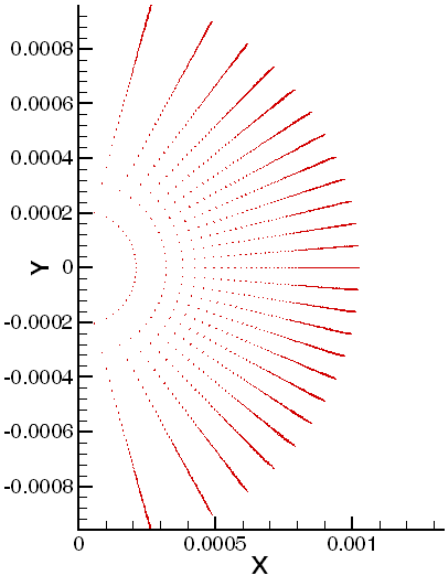

Figure 3. Flow field corresponding to Figure 2 after 0.1 seconds (2.5% total burning history)

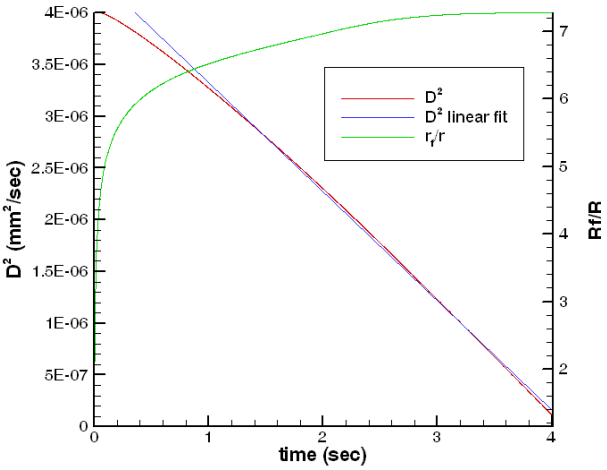

Figure 4. Burning history for 1 mm initial radius droplet with initial Peclet number of 4.

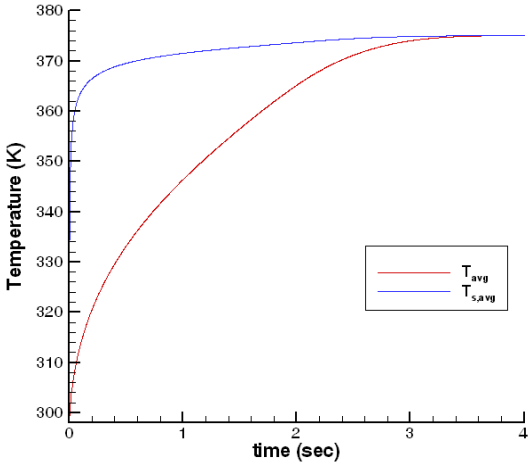

Figure 5. Surface temperature and droplet average temperature history for 1 mm initial radius droplet with initial Peclet number of 4

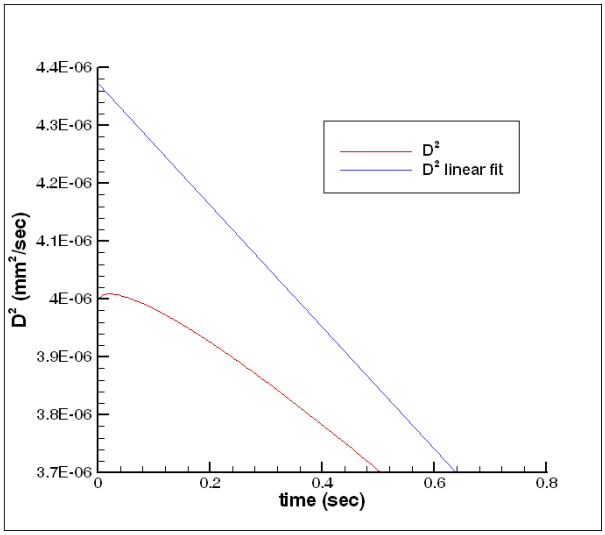

Figure 6. Burning history for 1 mm initial radius droplet with initial Peclet number of 4. Note initial increase in droplet diameter associated with thermal expansion.